# Control of a Back-to-Back Two-Level/Five-Level Grid Connection of a Wind Turbine

Mohammed Y. Marouf[1], Mohammed K. Fellah[1], Mohammed Yaichi[2], Mohammed F. Benkhoris[3]
1- ICEPS Laboratory (Intelligent Control and Electrical Power System), Djillali Liabes University of Sidi Bel-Abbes, Sidi Bel-Abbes, Algeria.
Email: maroufyasser@yahoo.fr (Corresponding author), Email: mkfellah@yahoo.fr
2- Photovoltaic Pumping Team, Research Unit in Renewable Energies in the Saharian Medium CDER, Adrar, Algeria.
Email : yaichi_mohammed@yahoo.fr
3- IREENA Laboratory, Ecole Polytechnique de Nantes, Nantes, France.
Email : mohamed-fouad.benkhoris@univ-nantes.fr

Received: January 2018 Revised: March 2018 Accepted: June 2018

**ABSTRACT:**
This paper proposes a new Space Vector Modulation (SVM) technique to control the grid-side inverter for improving the output power quality of a Doubly-Fed Induction Generator (DFIG) based Wind Energy Conversion System (WECS). A five-level Cascaded H-Bridge Inverter (CHBI) was used to connect the DFIG to the grid. The SVM algorithm enables controlling of the DFIG inverter which improves the quality of the output power by reducing the Total Harmonic Distortion (THD) of the generated currents and power ripples. However, the multi-level inverter has a major drawback, the even-order harmonics production, which can be overcame by controlling the five-level CHBI using this novel SVM technique generalized to N-level. The paper further presents the mechanism of this algorithm and a method to deduce the trajectories from the sequences, enabling reduction of the time and number of commutations, a better performance among several possible trajectories, and reduction of the THD rate of the DFIG output currents.

**KEYWORDS:** Wind Energy Conversion System, Doubly-Fed Induction Generator, Five-Level Inverter, Space Vector Modulation, Total Harmonic Distortion.

## 1. INTRODUCTION

A rapid development in the wind-energy industry has necessitated the improvement of methods and materials used to take advantage of this kind of energy. Wind energy is the safest, simplest, and most efficient method for achieving a balance between energy production and demand. Moreover, it does not produce any greenhouse gases. Electricity produced using wind energy reduces the yearly $CO_2$ emission by 0.8 to 0.9 tons compared with thermal power generation. Wind energy generators are primarily composed of metal, composites, and polymers and do not produce radioactive or toxic waste [1].

Recently, several studies have been conducted to improve the output power of wind energy conversion systems (WECSs). N. Vlastimir *et al.* [2] studied the design of an innovative wind turbine system. The theory of inventive problem solving was used as a systematic method to provide conceptual designs of wind turbines and improve the capability of developing innovative products. Y. Djeriri *et al.* [3] used a three-level neutral-point-clamped converter based on direct power control to manage the power generation of a doubly-fed induction generator (DFIG) and reduce the total harmonic distortion (THD) rate of the output current. O. Aouchenni et al. [4] carried out a theoretical study of a wind farm based on doubly-fed induction generator (DFIG) connected to the grid through a five-level neutral point clamped inverter. They proposed a DC filter model in order to maintain the DC voltage constant in each capacitor and to avoid the overvoltage of the inverter semiconductors. This topology was used to improve the voltage waveform and the quality of the power injected into the grid by reducing the total harmonics distortion (THD). R. C. John et al. [5] used a hybrid cascaded asymmetric inverter to control the output voltage of wind turbines and improve the output voltage spectrum. B. Naik et al. [6] used a pulse width modulation technique to control the output voltage of the cascaded H-bridge inverter (CHBI) connected to a single DC source-based WECS. D. Petković et al. [7] studied an adaptive neuro-fuzzy maximal power extraction of wind turbines with a continuous variable transmission by using benchmark data and Simulink.

Moreover, the adaptive neuro-fuzzy approach was investigated for wind turbine power coefficient estimation by using vibration data and MATLAB [8]. Recently, various studies [9-13] have used the space vector modulation (SVM) strategy to control the switches of different configurations and topologies of multilevel and multicellular inverters.

In this paper, the proposed method focuses on grid connection of the WECS by employing a back-to-back two-level/five-level grid connection topology to control and improve the output power quality of DFIG. The proposed grid connection system uses a two-level rectifier (generator side) combined with a five-level CHBI (grid-side) (Fig. 1). In this study, a novel SVM algorithm generalized to *N*-level was used to control the five-level inverter. This algorithm allows a reduction in the number of commutation and the switching losses in the inverter. Consequently, all even-order harmonics of the output current are eliminated, and a considerable flexibility can be obtained to optimize the switching waveforms. This configuration (back-to-back two-level/five-level grid connection topology combined with the new SVM technique) was particularly designed to reduce the current THD and power ripples of the DFIG.

The current and total voltage stresses were divided through the switches and the input voltage was split into several fractions to decrease the power switches rate. Thus, conventional semiconductors can be used to manage the high output power of the DFIG. This SVM algorithm was studied in detail by [11, 15, 16] and applied to control the stacked multicellular inverters and five-level inverters.

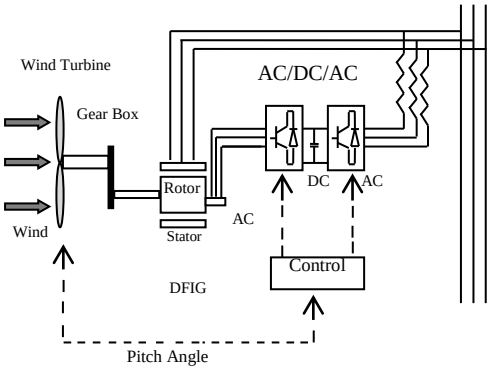


**Fig. 1.** WECS based on the DFIG.

## 2. OVERVIEW OF THE SYSTEM

The multilevel inverter was introduced in the market to overcome the difficulties encountered while connecting a single-power semiconductor switch directly to a medium-voltage grid [19] and to operate at higher voltage levels. The system details are as follows:

### 2.1. Generator-side Rectifier:

The generator-side rectifier was directly connected to the DFIG stator. Park transformation was used to transform the DFIG equations into the reference frame of Park [5]. A distinguished and proven universal bridge or a three-phase six-pulse full-diode bridge rectifier was used to convert the DFIG output power from AC to DC. A DC capacitor was connected as a filter to the output terminals of the three-phase rectifier.

### 2.2. Grid-side Inverter:

The grid-side inverter must be controlled to ensure that the active-generated power is fed back to the grid and the DC-link voltage is maintained constant [4, 5, 20]. Multilevel inverters are advantageous due to their DC-link utilization, power quality, and high efficiency of more than 95% at a nominal operating point. Using the five-level three-phase CHBI with this SVM algorithm [16] improved the quality of the DFIG output power and reduced the THD rate. This converter comprised a series connection of a two four-quadrant converter by phase [6] to control the DFIG output power.

Fig. 2 shows the proposed system and the modifications on the grid-side inverter.

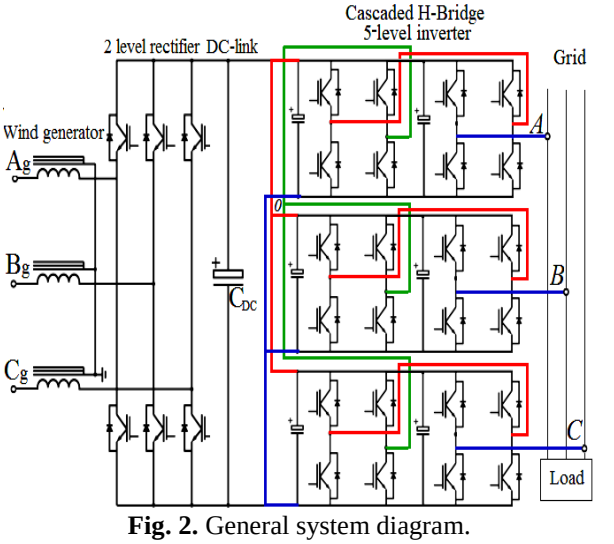


**Fig. 2.** General system diagram.

## 3. MODELING OF THE WIND TURBINE

The relation between the mechanical power of the wind turbine and wind speed [3] can be expressed using the following equations:

$$P_t = 1/2.\rho.R^2.v^3.C_p(\lambda,\beta) \quad (1)$$

$$\lambda = \Omega_r.R/v \quad (2)$$

Where λ, $C_p$ and β are the tip speed ratio, the power coefficient, and the pitch angle (degrees), respectively.

$R$ is the wind turbine radius; $v$ is the wind velocity (m/s); $\Omega_r$ is the turbine speed (rad/s); and $\rho$ is the air density (1.225 kg/m$^3$ at T = 15 °C).
$C_p$ can be modeled using the following generic equation:

$$C_p = f(\lambda,\beta) = C_1.\left(\frac{C_2}{\lambda_i} - C_3.\beta - C_4\right)\exp\left(\frac{-C_5}{\lambda_i}\right) + C_6.\lambda \qquad (3)$$

$$\frac{1}{\lambda_i} = \frac{1}{\lambda + 0.08\beta} - \frac{0.035}{\beta^3 + 1} \qquad (4)$$

The values of coefficients $C_1$ to $C_6$ are: $C_1$ =0.5176, $C_2$= 116, $C_3$=0.4, $C_4$=5, $C_5$=21, and $C_6$= 0.0068.

The torque coefficient ($C_t$) can be modeled using the following equation:

$$C_t = C_p/\lambda \qquad (5)$$

The produced torque can be given by using the following equation:

$$T_t = P_t/\Omega_r = 1/2.\rho.\pi.R^3.V^2.C_t(\lambda,\beta) \qquad (6)$$

The theoretical maximum power efficiency of any horizontal-axis wind turbine is approximately 16/27 ≈ 0.593, indicating that the wind turbine can extract a maximum of 59.3% of the wind energy [3]. This limit is termed as the Betz limit, which is defined as the maximum ratio between the mechanical power of the wind turbine and kinetic energy of the wind used to turn the rotor of the generator [18]. For real-time applications, this ratio ranges from 0.40 to 0.50.

Fig. 3. (a) and (b) show the behavior of the power coefficient ($C_p$) and the torque coefficient ($C_t$) according to the tip speed ratio (λ), respectively, for different values of the pitch angle (β).

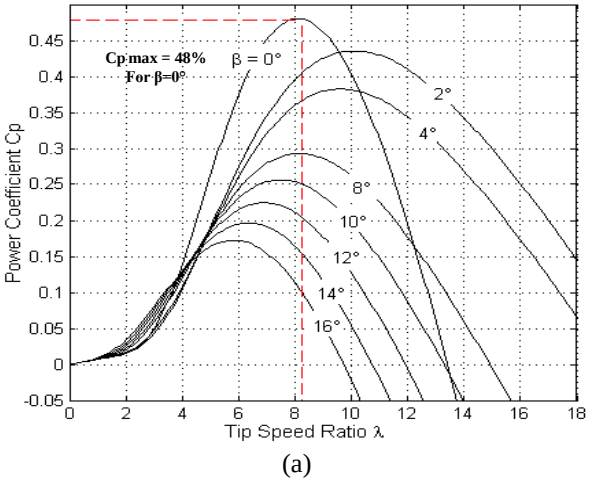


(a)

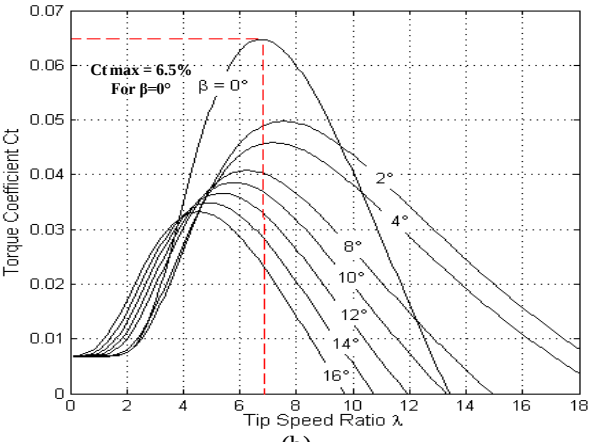


(b)

**Fig. 3.** Influence of pitch angle on the power coefficient (a) and torque coefficient (b).

## 4. MODELING THE DOUBLY-FED INDUCTION GENERATOR

In the *d-q* reference frame, the equations of the stator and rotor voltage of the DFIG can be given as follows:

$$\begin{Bmatrix} V_{ds} = R_s\, i_{ds} - \omega_s\, \varphi_{ds} + \tau\, \varphi_{ds} \\ V_{qs} = R_s\, i_{qs} - \omega_s\, \varphi_{qs} + \tau\, \varphi_{qs} \end{Bmatrix} \qquad (7)$$

$$\begin{Bmatrix} V_{dr} = R_r\, i_{dr} - (\omega_s - \omega_r)\varphi_{qr} + \tau\, \varphi_{dr} \\ V_{qr} = R_r\, i_{qr} - (\omega_s - \omega_r)\varphi_{dr} + \tau\, \varphi_{qr} \end{Bmatrix} \qquad (8)$$

where τ is the derivative symbol ($d/d_t$).

The stator and rotor flux components can be expressed as follows in the *d-q* frame:

$$\begin{Bmatrix} \varphi_{ds} = (L_{is} + L_m) i_{ds} + L_m\, i_{dr} = L_s\, i_{ds} + L_m\, i_{dr} \\ \varphi_{qs} = (L_{is} + L_m) i_{qs} + L_m\, i_{qr} = L_s\, i_{qs} + L_m\, i_{qr} \end{Bmatrix} \qquad (9)$$

$$\begin{Bmatrix} \varphi_{dr} = (L_{ir} + L_m) i_{dr} + L_m\, i_{ds} = L_s\, i_{dr} + L_m\, i_{ds} \\ \varphi_{qr} = (L_{ir} + L_m) i_{qr} + L_m\, i_{qs} = L_r\, i_{qr} + L_m\, i_{qs} \end{Bmatrix} \qquad (10)$$

Where,

$$L_s = L_{is} + L_m \qquad (11)$$

$$L_r = L_{ir} + L_m \qquad (12)$$

The electromagnetic torque of the DFIG is expressed by,

$$T_{em} = -3/2\, p(L_m/L_r)(\varphi_{ds}\, i_{qr} - \varphi_{qs}\, i_{dr}) \qquad (13)$$

The mechanical equation can be expressed as follows:

$$T_t = T_{em} + J\tau\Omega_r + f_r\Omega_r \quad (14)$$

The active and reactive power equations of the grid side are expressed as follows:

$$\begin{cases} P_S = 3/2\left(V_{ds}i_{ds} + V_{qs}i_{qs}\right) \\ Q_S = 3/2\left(V_{qs}i_{ds} + V_{ds}i_{qs}\right) \end{cases} \quad (15)$$

## 5. SVM CONTROL OF THE FIVE-LEVEL THREE-PHASE CASCADED H-BRIDGE INVERTER

The five-level three-phase CHBI was connected to the output of the rectifier after the filtering capacitor. Each single-phase of the H-bridge was independently supplied with a single DC voltage. The output of the inverter was directly connected to the grid (Fig. 2).

The use of this command in digital signal processors and microprocessors is difficult due to an increase in the number of levels of the SVM-controlled multilevel inverters. For very high levels, implementing these SVM algorithms in such processors is difficult. Furthermore, the SVM command is a nonstandard adaptive control technique [7, 8], which indicates that each time the number of levels for the inverter changes, the SVM control algorithm also changes, causing difficulties in implementing the multilevel vector modulation [17].

An efficient SVM algorithm was presented to solve these problems. This algorithm allowed controlling the three-phase five-level CHBI to improve the quality of the DFIG output power. Generalized to *N*-level, this algorithm was based on coordinate transformation, detection of the three closest vectors, and the calculation of the switches commutation time.

The following section explains the mechanisms of the SVM technique and methods to deduce the trajectories from the sequences that provide a better performance among several possible trajectories. This technique was used for the application of two particular trajectories [14, 16].

### 5.1. Switching States and Representation of Switching Vectors: [9, 11, 17]

The multilevel inverter is a voltage synthesizer that produces several discrete voltage levels from using its own voltage [17]. Furthermore, although numbering the switching states is a more general approach, the equivalent nomination where 2, 1, and 0 are denoted by p, o, and n, respectively, is more common for the multilevel inverter. However, both can be used. The output switching state of a phase for a five-level inverter takes the numbers 0, 1, 2, 3 and 4.

Fig. 4 shows the space vector diagram of the five-level inverter with the corresponding switching states [16].

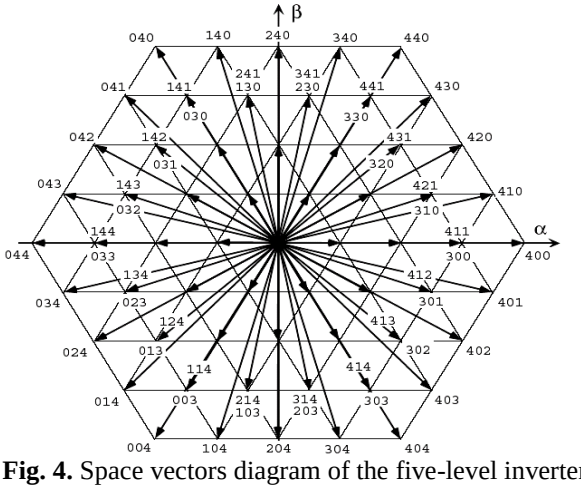


**Fig. 4.** Space vectors diagram of the five-level inverter.

The SVM approach is perhaps the most powerful technique because it offers more freedom to control and optimize switching models than any other modulation approach [11]. This approach provides a significant flexibility to improve switching schemes [9]. However, converters with a higher number of levels make real-time execution difficult [17]. Therefore, the first major task of this study was to simplify and generalize the execution of the SVM for the grid-side inverter of the DFIG by using a simple, robust, fast, and efficient algorithm for *N*-level inverters, which can be used with any real-time processor available in the market and employed for renewable energy sources. In the two-level inverter simplest hexagon, a new ring is added with each new level in an equilateral triangle way, creating a new hexagon of voltage vectors (Fig. 5). This basic principle helped establish this algorithm.

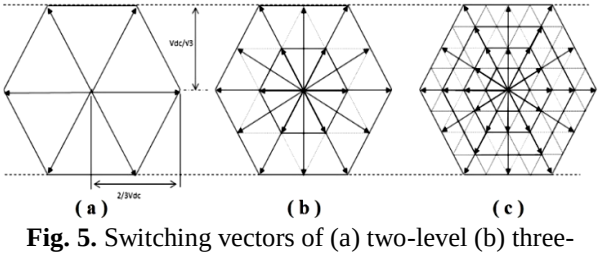


**Fig. 5.** Switching vectors of (a) two-level (b) three-level, and (c) five-level inverters.

This regularity in the structure of the hexagons can be used to efficiently represent the vectors in the plane and generalize the SVM algorithm [11]. To use the symmetrical structure of hexagons, a set of nonorthogonal vectors can be selected for a new base (*g*, *h*), where the switching and reference vector can be represented.

This base change [11] is defined by,

$$\left\{\vec{g}(v_{ab},v_{bc},v_{ca}),\vec{h}(v_{ab},v_{bc},v_{ca})\right\}=\left\{\begin{bmatrix}U\\0\\-U\end{bmatrix},\begin{bmatrix}0\\U\\-U\end{bmatrix}\right\} \quad (16)$$

where $U$ is the DC-link voltage.

### 5.2. Coordinate Transformation: [14-16]

The first step in the algorithm is to transform the reference vector $\overrightarrow{V_{ref}}$ into a two-dimensional coordinate system. This can be achieved using a linear base change transformation. Thus, the transformation matrix differs in accordance with the source coordinate system, which can be expressed as follows:

$$\overrightarrow{V_{ref(g,h)}}=T.\overrightarrow{V_{ref(v_{ab},v_{bc},v_{ac})}} \quad (17)$$

where,

$$\begin{bmatrix}V_a\\V_b\\V_c\end{bmatrix}=r\begin{bmatrix}\cos(\omega t)\\\cos(\omega t-2\pi/3)\\\cos(\omega t+2\pi/3)\end{bmatrix} \quad (18)$$

$$\text{And } T=1/3.(N-1)/2.\begin{bmatrix}2&-1&-1\\-1&2&-1\end{bmatrix} \quad (19)$$

Fig. 6 shows the corresponding switching states of the five-level inverter in the new two-dimensional reference frame ($g$, $h$) ($\overrightarrow{M_{REF}}$ is the switching state vector).

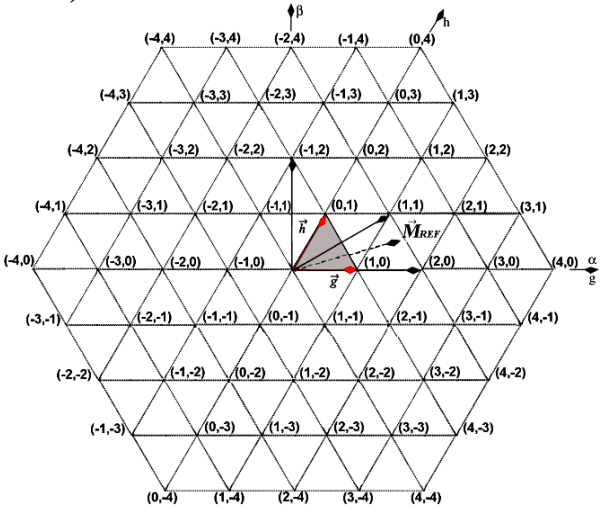


**Fig. 6.** Switching state vectors of the three-level inverter in the ($g$, $h$) system.

Most commands of AC machines were operated in a two-phase reference frame, which can be achieved by transforming the reference vector from (α, β) to ($g$, $h$) by using the base change transformation [12]. The result of the matrix transformation is as follows:

$$\overrightarrow{V_{ref(g,h)}}=T_1.\overrightarrow{V_{ref(\alpha,\beta)}} \quad (20)$$

$$T_1=3/2.(N-1)/2.\begin{bmatrix}1&-1/\sqrt{3}\\0&2/\sqrt{3}\end{bmatrix} \quad (21)$$

### 5.3. Detection of the Closest Three Vectors:

The switching vectors have an integer coordinate number, which is advantageous because the four closest vectors to the reference vector can be identified easily. However, the calculation of the vectors whose coordinates are combinations of the rounded superior and inferior values of the reference vector number is as follows [10, 14, 15]:

$$\begin{aligned}\overrightarrow{V_{ul}}&=\begin{bmatrix}\lceil V''_{refg}\rceil\\\lfloor V'_{refh}\rfloor\end{bmatrix},\overrightarrow{V_{lu}}=\begin{bmatrix}\lfloor V'_{refg}\rfloor\\\lceil V''_{refh}\rceil\end{bmatrix},\\\overrightarrow{V_{uu}}&=\begin{bmatrix}\lceil V''_{refg}\rceil\\\lceil V''_{refh}\rceil\end{bmatrix},\overrightarrow{V_{ll}}=\begin{bmatrix}\lfloor V'_{refg}\rfloor\\\lfloor V'_{refh}\rfloor\end{bmatrix},\end{aligned} \quad (22)$$

Where $\lceil V''_{ref}\rceil$ : indicates the superior rounded value of $V_{ref}$

$\lfloor V'_{ref}\rfloor$: indicates the inferior rounded value of $V_{ref}$.

The endpoints of the four closest vectors formed an equal parallelogram, which was divided into two equilateral triangles by the diagonal connecting the vectors $\overrightarrow{V_{ul}}$ and $\overrightarrow{V_{lu}}$. Vectors $\overrightarrow{V_{ul}}$ and $\overrightarrow{V_{lu}}$ were still two of the three closest vectors [15]. The third closest vector, considered as a reference, was one of the two remaining vectors located on the same side of the diagonal $g+h=V_{ulg}+V_{ulh}$. Therefore, the third closest vector can be determined by evaluating the sign of the expression:

$$V_{refg}+V_{refh}-(V_{ulg}+V_{ulh}) \quad (23)$$

If the sign is positive, the vector $\overrightarrow{V_{uu}}$ is considered to be the third closest vector, otherwise, the vector $\overrightarrow{V_{ll}}$ is the closest one. Thus, closest three vectors for $N$-level inverters are identified.

Fig. 7 shows the method to obtain the closest three vector.

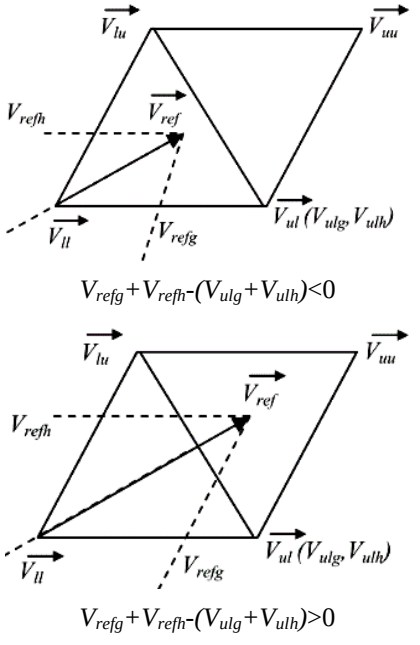


**Fig. 7.** Method to obtain the three closest vectors (reference vector position) in two different cases of the same four closest vectors.

### 5.4. Calculation of the Switching Time: [15]

Upon identifying the three closest vectors, the commutations times of the switches can be determined by solving (24) and (25).

$$\overrightarrow{V_{ref}} = \left(d_1.\overrightarrow{V_1} + d_2.\overrightarrow{V_2} + d_3.\overrightarrow{V_3}\right) \tag{24}$$

With the following additional constraint on the conduction times:

$$d_1 + d_2 + d_3 = 1 \tag{25}$$

where, $\overrightarrow{V_1} = \overrightarrow{V_{ul}}; \overrightarrow{V_2} = \overrightarrow{V_{lu}}; \overrightarrow{V_3} = \overrightarrow{V_{ll}}$ or $\overrightarrow{V_3} = \overrightarrow{V_{uu}}$

Solutions are the parts of the $V_{ref}$ coordinates [19] because all switching vectors always have integer coordinates.

$$\text{If: } \overrightarrow{V_3} = \overrightarrow{V_{ll}} \text{ so } \begin{Bmatrix} d_{ul} = V_{refg} - V_{llg} \\ d_{lu} = V_{refh} - V_{llh} \\ d_{ll} = 1 - d_{ul} - d_{lu} \end{Bmatrix} \tag{26}$$

Or:

$$\text{If: } \overrightarrow{V_3} = \overrightarrow{V_{uu}} \text{ so } \begin{Bmatrix} d_{ul} = V_{refh} - V_{uuh} \\ d_{lu} = V_{refg} - V_{uug} \\ d_{uu} = 1 - d_{ul} - d_{lu} \end{Bmatrix} \tag{27}$$

Then, this method and the algorithm are used to control the five-level CHBI connected to the DFIG after the rectifier and the DC-link. The simulation results are presented in the following section.

## 6. SIMULATION RESULTS AND DISCUSSION

This section explains and discusses the performances of a 1.5-MW DFIG connected to the grid using the five-level CHBI which is controlled by the proposed SVM algorithm. The control scheme and SVM control strategy of the five-level inverter connected to the grid (grid side) of the wind turbine were simulated and tested in terms of power, current, and harmonic distortion. Furthermore, the performance, reliability, and robustness of the system were examined at a super-synchronous speed.

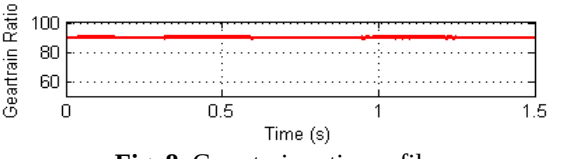


**Fig. 8**. Gear-train ratio profile.

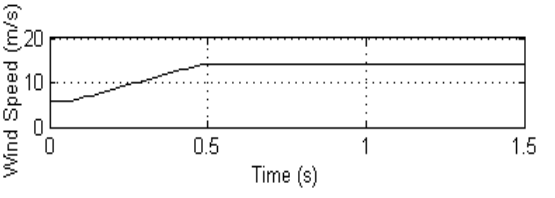


**Fig. 9**. Wind speed variation.

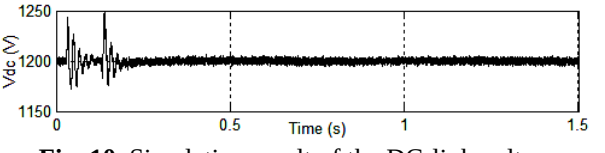


**Fig. 10**. Simulation result of the DC-link voltage.

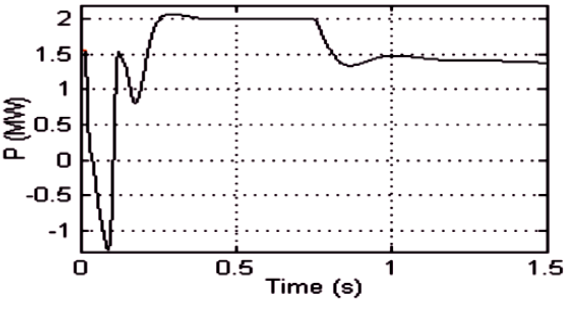


(a): Simulation result of the active power.

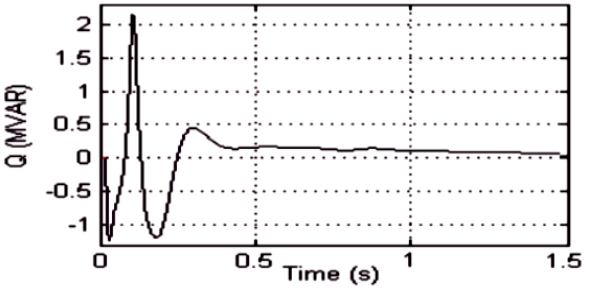


(b): Simulation result of the reactive power.

**Fig. 11**. Simulation results of the DFIG power.

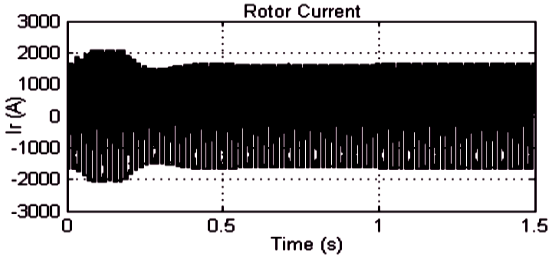


(a)Simulation result of the rotor current.

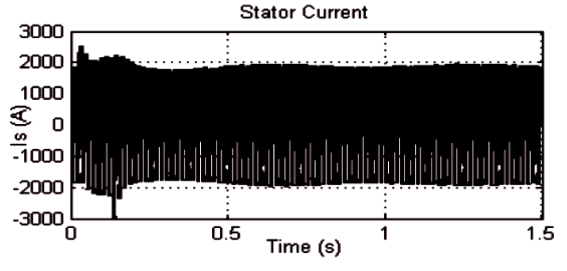


(b)Simulation result of the stator current.

**Fig. 12**. Simulation result of the DFIG current.

Fig. 8 presents the gear-train ratio (fixed at 90) of the wind turbine.

Fig. 9 shows the variation of the wind speed. The speed was initially set at 6 m/s; however, at t = 0.1 s, the speed increased abruptly to 14 m/s and then became constant.

Fig. 10 shows the DC-link voltage at the output of the rectifier. During the interval 0 s < t < 0.25 s, the DC voltage was unstable, varying between 1175 and 1250 V. This variation was due to the instability of the voltage delivered by the generator in the same time interval. The DC voltage stabilized at approximately 1200 V.

Fig. 11 (a) and (b) show the progression of the active and reactive power, respectively. For time interval 0s < t < 0.1s, the two powers were observed to be unbalanced and unstable. The active power decreased from 1.5 MW to –1.4 MW, whereas the reactive power increased from –1.3 MVAR to 2.2 MWAR. This change was observed because the wind turbine absorbed the nominal power required by the wind generator mechanisms to constrain not only the mechanical forces for repositioning the nacelle but also the orientation and rotation initiation of the blades of the wind turbine. For the time interval 0.1 s < t < 0.3 s, the active power increased smoothly with the increasing wind speed, and the reactive power decreased simultaneously to a negative value, after which both powers stabilized. The active power stabilized at approximately 1.5 MW at t = 0.75 s, whereas the reactive power stabilized at approximately 0 MVAR (reference value) at t = 0.4 s. Furthermore, Fig. 11 (a) and (b) demonstrate that the new SVM algorithm can control the active and reactive powers of DFIG with a very fast response time and no errors.

Fig. 12 (a) and (b) indicate that the stator and rotor currents were suitable sinusoidal signals, which stabilized at a steady state at approximately t = 0.5 s.

The fast Fourier transform analyzer on the stator current waveform ($I_{s\alpha}$) delivered to the grid was used to determine the THD rate (Fig. 13) and observe the features of the control strategy (new SVM algorithm to control the five-level CHBI connected to the grid side of the DFIG). The results are as follows:

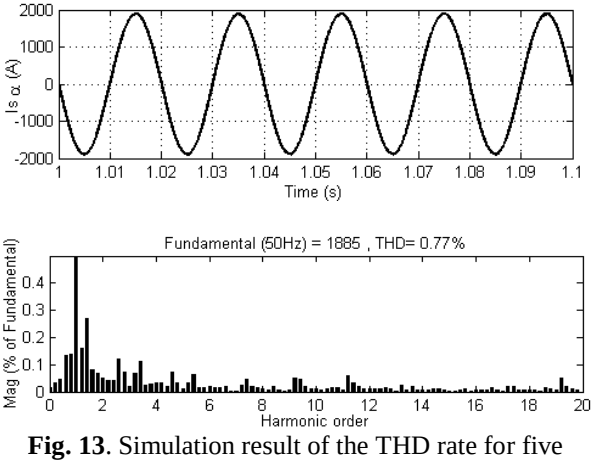


**Fig. 13**. Simulation result of the THD rate for five cycles starting at t = 1s.

A satisfactory current waveform was obtained without using any filter. The THD rate of the output stator current, as shown in Fig. 13, was 0.77%, indicating the reliability and effectiveness of this control technique.

## 7. CONCLUSION

This paper presents an improvement in the quality of the DFIG output power in the WECS by using the new SVM technique applied to the five-level CHBI that was connected to the grid-side of the DFIG. The study and simulation were presented to optimize and improve the quality of the DFIG output power by reducing the

power ripples and THD rate of the output current, which consequently reduced the transitional regime time and stabilized the system in a short time.

The SVM algorithm was generalized to the *N*-level, allowing the elimination of all even-order harmonics, to reduce the time and number of commutations, to have better performance among several possible trajectories, and reduce the THD rate of the output currents.

The five-level CHBI with the SVM algorithm exhibited satisfying results, provided a steady-state performance and improved the output waveforms of the inverter signals with a very fast response time. Moreover, it improved the power quality with a substantial reduction of 0.77% of the THD compared with that in previous studies.

This method can be used in the WECS. Further improvements can be performed by testing this SVM algorithm with other topologies.

## APPENDIX

**Table 1.** Simulation parameters.

| Doubly-fed induction generator parameters | |
|---|---|
| Rated Power, Pn | 1.5 MW |
| Stator rated voltage, Vs | 690V |
| Rated Current, In | 1900A |
| Rated DC-Link voltage, Udc | 1200V |
| Stator rated frequency f | 50 Hz |
| Number of pair of poles, p | 2 |
| Rotor inductance, Rr | 0.021Ω |
| Stator inductance, Rs | 0.012 Ω |
| Mutual inductance, Lm | 0.0135 H |
| Rotor inductance, Lr | 0.0136 H |
| Stator Inductance, Ls | 0.0137H |
| Wind turbine parameters | |
| Wind turbine blade radius, R | 35.25 m |
| Number of Wind turbine blades | 3 |
| Gearbox ratio, G | 90 |
| Moment of inertia, J | 1000 kg.m² |
| Viscous friction coefficient, fr | 0.0024 N.m/s |
| Cut-in wind speed | 6 m/s |
| Cut-out wind speed | 26 m/s |
| Nominal wind speed, V | 14 m/s |

## REFERENCES.


[1] M. Khechana, M. Nadjah and L. Laiche, **"Etude De La Nacelle Et Du Mat D'une Eolienne De Faible Puissance**," *Revue des Energies Renouvelables*, CISM'08 Oum El Bouaghi, pp. 195–203, 2008.

[2] V. Nikolić, S. Sajjadi, D. Petković, S. Shamshirband, Ž. Ćojbašić, and L. Y. Por, **"Design And State Of Art Of Innovative Wind Turbine Systems**," *Renewable and Sustainable Energy Reviews*, Vol. 61, pp. 258–265, 2016.

[3] Y. Djeriri, A. Meroufel, and B. Belabbes, **"Three-Level NPV Voltage Source Converter Based Direct Power Control Of The Doubly Fed Induction Generator At Low Constant Switching Frequency,"** *Revue des Energies Renouvelables*, Vol. 16, *1*, pp. 91–103, 2013.

[4] O. Aouchenni, R. Babouri, K. Ghedamsi, and D. Aouzellag, **"Wind Farm Based On Doubly Fed Induction Generator Entirely Interfaced with Power Grid through Multilevel Inverter**," *Rev. Roum. Sci. Techn.–Électrotechn. et Énerg*, Vol. 62, *2*, pp. 170–174, 2017.

[5] R. C. John, P. V. J. Sebastian, and R. Mahalaksmi, **"Cascaded Asymmetric Multilevel Inverter for Wind Energy Conversion System**," *International Journal for Research and Development in Engineering (IJRDE)*, Vol. 2, pp. 24–28, 2013.

[6] B. Naik, M. Behera, and B. Mohapatra, **"Wind Energy Conversion based on Cascaded H-Bridge Inverter using Single DC source**," *International Conference on Emergent Trends in Computing and Communication (ETCC)*, pp. 1–5, 2015.

[7] D. Petković, Ž. Ćojbašić, V. Nikolić, S. Shamshirband, M. L. M. Kiah, N. B. Anuar, and A. W. A. Wahab, **"Adaptive Neuro-Fuzzy Maximal Power Extraction of Wind Turbine With Continuously Variable Transmission,"** *Energy*, Vol. 64, pp. 868–874, 2014.

[8] D. Petković, Ž. Ćojbašič, and V. Nikolić, **"Adaptive Neuro-Fuzzy Approach for Wind Turbine Power Coefficient Estimation**," *Renewable and Sustainable Energy Reviews*, Vol. 28, pp. 191–195, 2013.

[9] G. Gateau, T. Meynard, and L. Delmas, **"Stacked Multicellular Converter (SMC): Topology and Control**," *EPE Journal*, Vol. 12, *2*, pp. 14–18, 2002.

[10] K. Mathew, K. Gopakumar, and J. Mathew, **"Multilevel Octadecagonal Space Vector Generation for Induction Motor Drives By Cascading Asymmetric Three Level Inverters**," *IECON-38th Annual Conference on IEEE Industrial Electronics Society*, pp. 1915–1920, 2012.

[11] N. Celanovic, **"Space Vector Modulation And Control of Multilevel Converters**," *PhD thesis, Virginia Polytechnic Institute and State University*, USA, 2000.

[12] N. Celanovic, and D. Boroyevich, **"A Fast Space-Vector Modulation Algorithm for Multilevel Three-Phase Converters,"** *IEEE transactions on industry applications*, Vol. 37, *2*, pp. 637–641, 2001.

[13] J. Hawley, and X. Zhou, **"Space Vector Modulation in Multilevel Applications,"** *0-7803-7754-0/03/$17.00* © IEEE, 2003.

[14] S. Hanafi, M. K. Fellah, M. Yaichi, and M. F. Benkhoris, **"Nonlinear Feedback Decoupling Control Applied to Stacked Multicellular Converter,"** *Rev. Roum. Sci. Techn.–Électrotechn. et Énerg*, Vol. 59, 1, pp. 97–106, 2014.

[15] S. Hanafi, M. K. Fellah, M. Yaichi, and M. F. Benkhoris, **"Control of Stacked Multicellular Inverter,"** *Rev. Roum. Sci. Techn.–Électrotechn. et Énerg*, Vol. 12, pp. 278–282, 2016.

[16] M. Yaichi, and M. K. Fellah, **"An Implementation Mechanisms of SVM Control Strategies Applied to Five Levels Cascaded Multi-Level Inverters,"** *International Journal of Power Electronics and Drive Systems*, Vol. 4, 2, pp. 146, 2014.

[17] M. Flitti, M. K. Fellah, M. Yaichi, M. Khatir, and M. F. Benkhoris, **"Control Design Of Statcom using Five Level Neutral Point Clamped Converter And Its Application To Reactive Power,"** *Rev. Roum. Sci. Techn.–Électrotechn. et Énerg*, Vol. 59, 4, pp. 351–360, 2014.

[18] E. Hau, **"Wind Turbine Costs,"** *Wind Turbines, Springer Berlin Heidelberg*, pp. 789–843, 2013.

[19] P. V. V. N. M. Kumar, P. M. Kishore, and R. K. Nema, **"Simulation of Cascaded H-Bridge Multilevel Inverters for PV Applications,"** *Int. J. Chem. Tech. Res*, Vol. 5, 2, pp. 918–924, 2013.

[20] S. M. Muyeen, R. Takahashi, and T. Murata, **"A Variable Speed Wind Turbine Control Strategy to Meet Wind Farm Grid Code Requirements,"** *IEEE Transactions on power systems*, Vol. 25, *1*, pp. 331–340, 2010.